

November 2, 2018
hep-ph/01xxx

Complete next-to-leading order QCD corrections to charged Higgs boson associated production with top quark at the CERN Large Hadron Collider

SHOU-HUA ZHU

*Ottawa-Carleton Institute for Physics, Department of Physics, Carleton University,
Ottawa, Canada K1S 5B6*

The complete next-to-leading order (NLO) QCD corrections to charged Higgs boson associated production with top quark through $bg \rightarrow tH^-$ at the CERN Large Hadron Collider are calculated in the minimal supersymmetric standard model (MSSM) and two-Higgs-doublet model in the \overline{MS} scheme. The NLO QCD corrections can reduce the scale dependence of the leading order (LO) cross section. The K-factor (defined as the ratio of the NLO cross section to the LO one) does not depend on $\tan \beta$ if the same quark running masses are used in the NLO and LO cross sections, and varies roughly from ~ 1.6 to ~ 1.8 when charged Higgs boson mass increases from 200 GeV to 1000 GeV.

I. INTRODUCTION

The detection of the Higgs particles is one of the most important objectives of the Large Hadron Collider (LHC). Charged Higgs bosons are predicted in extended versions of the Standard model (SM), like two-Higgs-doublet models (2HDM) and the Minimal Supersymmetric Standard Model (MSSM). Discovery of such an additional charged Higgs boson will immediately indicate physics beyond the SM, unlike the case of the neutral Higgs boson. Hence, there is strong theoretical and experimental motivation for exploring the mechanisms of the charged Higgs boson production.

The charged Higgs boson H^\pm could appear as the decay product of primarily produced top quarks if the mass of H^\pm is smaller than $m_t - m_b$. For heavier H^\pm , the direct H^\pm production mechanisms at hadron colliders have been extensively investigated. At the LHC, the primary charged Higgs boson production channel is $gb \rightarrow H^- t$ [1] *. The study [3,4] shows that this production mechanism can be used to explore the parameter space of MSSM for m_{H^\pm} up to 1 TeV and $\tan\beta$ down to at least ~ 3 , and potentially to ~ 1.5 . Therefore, it is necessary to calculate and implement also the loop contributions to $gb \rightarrow H^- t$ for more accurate theoretical predictions.

The production mechanism of the heavy charged Higgs boson with heavy top quark has been studied two decades ago [5]. In order to resum the possible large terms like $\log(Q^2/m_b^2)$, the bottom quark parton distribution function (PDF) is introduced. Although, there are some doubts about the bottom parton description [6], the detailed study on the $P_{T,b}$ distribution [7] argues that the bottom parton description is reliable for the inclusive tH^- production process at LHC.

In earlier literature, the contribution of the initial-gluon process $gg \rightarrow H^- t\bar{b}$, which is only part of the next-to-leading order (NLO) QCD corrections to $gb \rightarrow H^- t$, has been calculated [8]. The supersymmetric electroweak corrections arising from the quantum effects which are induced by potentially large Yukawa couplings from the Higgs sector and the chargino-top(bottom)-sbottom(stop) couplings, neutralino- top(bottom)-stop(sbottom)

*See Ref. [2] for the discussion on other charged Higgs boson production mechanisms.

couplings and charged Higgs-stop-sbottom couplings are also studied [1,9], which can give rise to a 15% reduction of the lowest-order result. In Ref. [10], the electro-weak corrections to the process are also discussed. After the submission of this paper, another calculation on the QCD correction appeared [7], in which the corresponding results seemed compatible with ours. The study on the SUSY-QCD effect for this process is also done [7,11]. In this paper, we would present the detailed and complete NLO QCD corrections to $gb \rightarrow H^-t$. We should note here that the results presented in this paper are for the process $bg \rightarrow tH^-$; they are the same for the charge conjugate process $\bar{b}g \rightarrow H^+\bar{t}$.

The arrangement of this paper is as follows. Section II contains the analytic results, and in Section III we present numerical examples and discuss the implications of our results. The lengthy expressions of the form factors are collected in the Appendix.

II. ANALYTIC EXPRESSIONS

Including the NLO QCD corrections, the cross sections for $PP \rightarrow tH^-X$ at the CERN LHC can be written as

$$\sigma = \sigma^{LO} + \sigma^{Vir} + \sigma^{Real}, \quad (1)$$

where σ^{LO} is the cross section at leading order (LO), σ^{Vir} and σ^{Real} are cross sections from NLO QCD corrections arising from virtual and real processes.

A. LO cross section

The Feynman diagrams for the charged Higgs boson production via $b(p_1)g(p_2) \rightarrow t(k_1)H^-(k_2)$ at the LO are shown in Fig.1. The amplitudes are created by use of Feynarts [13] and are handled with the help of FeynCalc [14]. As usual, we define the Mandelstam variables as

$$\begin{aligned} s &= (p_1 + p_2)^2 = (k_1 + k_2)^2, \\ t &= (p_1 - k_1)^2 = (p_2 - k_2)^2, \\ u &= (p_1 - k_2)^2 = (p_2 - k_1)^2. \end{aligned} \quad (2)$$

The amplitude at the LO could be written as

$$M_{LO} = \sum_{i=1}^6 t_i [c_1 M_{2i-1} + c_2 M_{2i}], \quad (3)$$

where the non-vanishing form factors are

$$\begin{aligned} t_2 &= \frac{1}{m_t^2 - u} - \frac{1}{s}, \\ t_3 &= \frac{2}{m_t^2 - u}, \\ t_5 &= -\frac{2}{s}, \end{aligned} \quad (4)$$

where $c_1 = \frac{g_w g_s \mu^{2\epsilon} m_b \tan \beta}{2\sqrt{2} m_w}$ and $c_2 = \frac{g_w g_s \mu^{2\epsilon} m_t \cot \beta}{2\sqrt{2} m_w}$. In Eq. (3) M_{2i} and M_{2i+1} ($i=1-6$) are the standard matrix elements which are defined as

$$\begin{aligned} M_1 &= \bar{u}(k_1) \not{\epsilon}(p_2) P_R u(p_1), \\ M_2 &= \bar{u}(k_1) \not{\epsilon}(p_2) P_L u(p_1), \\ M_3 &= \bar{u}(k_1) \not{p}_2 \not{\epsilon}(k_2) P_R u(p_1), \\ M_4 &= \bar{u}(k_1) \not{p}_2 \not{\epsilon}(k_2) P_L u(p_1), \\ M_5 &= \bar{u}(k_1) P_R u(p_1) k_1 \cdot \varepsilon(p_2), \\ M_6 &= \bar{u}(k_1) P_L u(p_1) k_1 \cdot \varepsilon(p_2), \\ M_7 &= \bar{u}(k_1) \not{p}_2 P_R u(p_1) k_1 \cdot \varepsilon(p_2), \\ M_8 &= \bar{u}(k_1) \not{p}_2 P_L u(p_1) k_1 \cdot \varepsilon(p_2), \\ M_9 &= \bar{u}(k_1) P_R u(p_1) p_1 \cdot \varepsilon(p_2), \\ M_{10} &= \bar{u}(k_1) P_L u(p_1) p_1 \cdot \varepsilon(p_2), \\ M_{11} &= \bar{u}(k_1) \not{p}_2 P_R u(p_1) p_1 \cdot \varepsilon(p_2), \\ M_{12} &= \bar{u}(k_1) \not{p}_2 P_L u(p_1) p_1 \cdot \varepsilon(p_2), \end{aligned} \quad (5)$$

where the color matrix T^a has been suppressed. In this paper, we perform the calculations in Feynman gauge and in d time-space dimensions with $d = 4 - 2\epsilon$. For simplicity, throughout the paper we omit the bottom quark dynamical mass but keep the mass-term only in Yukawa couplings. The discussion on the error induced by massless bottom quark approximation can be found in Ref. [12].

The LO cross section can then be written as

$$\frac{d\sigma_{LO}}{dx_1 dx_2} = d\hat{\sigma}^0 G_{b/A}(x_1, \mu_f) G_{g/B}(x_2, \mu_f) + [A \leftrightarrow B], \quad (6)$$

with

$$d\hat{\sigma}^0 = \frac{1}{24} \frac{1}{4(1-\epsilon)} \frac{1}{2s} |M_{LO}|^2 d\Phi_2 \quad (7)$$

where the factor $\frac{1}{24}$ and $\frac{1}{4(1-\epsilon)}$ are the color and spin average, respectively, and two-body phase space is

$$d\Phi_2 = \frac{1}{8\pi} \left(\frac{4\pi}{s} \right)^\epsilon \frac{1}{\Gamma(1-\epsilon)} \left[\lambda \left(1, \frac{m_{H^\pm}^2}{s}, \frac{m_t^2}{s} \right) \right]^{1/2-\epsilon} v^{-\epsilon} (1-v)^{-\epsilon} dv, \quad (8)$$

with $v = \frac{1}{2}(1 + \cos \theta)$, where θ is the center-of-mass scattering angle between p_1 and k_1 . Here λ is the two-body phase space function

$$\lambda(x, y, z) = x^2 + y^2 + z^2 - 2xy - 2xz - 2yz. \quad (9)$$

B. Virtual corrections

The Feynman diagrams for the NLO virtual corrections are shown in Fig. 2. The virtual diagrams with the self-energy insertions on the external legs are not shown. They can be obtained by inserting diagram (a)-(d) of Fig. 2 into the external legs of the LO diagrams in Fig. 1. At the same time, the diagrams containing counter-terms can be easily got by inserting corresponding counter-terms into external legs, internal propagators and vertex of the LO diagrams.

In order to remove the UV divergences, we have to renormalize the strong coupling constant, the Yukawa coupling constants, the quark masses and the wave functions of quarks and gluon. The strong coupling constant and the gluon wave function are renormalized in the \overline{MS} scheme as

$$\begin{aligned} \frac{\delta g_s}{g_s} &= -\frac{\alpha_s}{8\pi} \beta_0 \Delta, \\ Z_g &= -\frac{\alpha_s}{4\pi} (2C_A - \beta_0) \Delta, \end{aligned} \quad (10)$$

with $\Delta = \frac{1}{\epsilon} - \gamma_E + \log(4\pi)$, $\beta_0 = (11C_A - 2n_f)/3$, $C_A = 3$ and $C_F = 4/3$. Here, $n_f = 6$ is the number of fermions.

We renormalize wave function and mass of the bottom quark in the \overline{MS} scheme

$$\begin{aligned}\frac{\delta m_b}{m_b} &= -\frac{\alpha_s}{4\pi} 3C_F \Delta, \\ Z_b &= -\frac{\alpha_s}{4\pi} C_F \Delta.\end{aligned}\quad (11)$$

At the same time, we will renormalize the top quark mass in two schemes: on-mass-shell (OS) and \overline{MS} .

$$\begin{aligned}\frac{\delta m_t}{m_t} &= -\frac{\alpha_s}{4\pi} 3C_F \left[\Delta + \frac{4}{3} - \log(m_t^2/\mu^2) \right], \quad \text{in OS scheme} \\ \frac{\delta m_t}{m_t} &= -\frac{\alpha_s}{4\pi} 3C_F \Delta, \quad \text{in } \overline{MS} \text{ scheme}.\end{aligned}\quad (12)$$

Hereafter we will refer OS and \overline{MS} schemes to the different mass renormalization of the top quark. The comparison between the results in these two schemes will be discussed in the numerical section. The wave function renormalization constant of top quark is chosen the same with that of b quark

$$Z_t = -\frac{\alpha_s}{4\pi} C_F \Delta. \quad (13)$$

The renormalized virtual amplitude can then be written in the following way,

$$M_{\text{ren}} = M_A + M_B, \quad (14)$$

where M_A is the amplitude from the diagrams (e)-(o) of Fig. 2 and M_B is the amplitude from the diagrams which contain self-energy insertion on the external legs or counter-terms.

The M_A can be written as

$$M_A = \sum_{i=e}^o M_A^i, \quad (15)$$

where i represents the diagram index of Fig. 2. For each diagram i , we can generally write the amplitude as

$$M_A^i = \sum_{j=1}^6 f_j [c_1 M_{2i-1} + c_2 M_{2i}], \quad (16)$$

where the non-vanishing form factors f_j are given explicitly in Appendix and the M_j are the standard matrix elements given in the previous subsection.

The M_B can be written as

$$M_B = M_B^1 + M_B^2, \quad (17)$$

where

$$M_B^1 = M_{LO} \left\{ \frac{\delta g_s}{g_s} + \frac{Z_t}{2} + \frac{Z_b}{2} + \frac{Z_g}{2} + \frac{\alpha_s}{8\pi} \left[-3\Delta + \frac{14}{3} \log(m_t^2/\mu^2) - \frac{16}{3} \right] \right\}, \quad (18)$$

$$M_B^2 = \sum_{i=1}^6 [c_1 f_s^{2i-1} M_{2i-1} + c_2 f_s^{2i} M_{2i}]. \quad (19)$$

Here the non-vanishing form factors f_s^i ($i = 1 - 12$) are

$$\begin{aligned} f_s^1 &= f_s^2 = \frac{\delta m_t}{m_t^2 - u}, \\ f_s^3 &= \frac{-2m_t \delta m_t}{(m_t^2 - u)^2} + \frac{\delta m_b}{m_b} \left[\frac{1}{m_t^2 - u} - \frac{1}{s} \right], \\ f_s^4 &= \frac{-2m_t \delta m_t}{(m_t^2 - u)^2} + \frac{\delta m_t}{m_t} \left[\frac{1}{m_t^2 - u} - \frac{1}{s} \right], \\ f_s^5 &= 2 \left[\frac{-2m_t \delta m_t}{(m_t^2 - u)^2} + \frac{\delta m_b}{m_b} \frac{1}{m_t^2 - u} \right], \\ f_s^6 &= 2 \left[\frac{-2m_t \delta m_t}{(m_t^2 - u)^2} + \frac{\delta m_t}{m_t} \frac{1}{m_t^2 - u} \right], \\ f_s^9 &= -\frac{2}{s} \frac{\delta m_b}{m_b}, \\ f_s^{10} &= -\frac{2}{s} \frac{\delta m_t}{m_t}. \end{aligned} \quad (20)$$

After squaring the renormalized amplitude and performing the spin and color summations, the partonic cross section with virtual corrections can be written as

$$\frac{d\sigma^{Vir}}{dx_1 dx_2} = 2 \operatorname{Re} \left[\overline{\sum} (M_{\text{ren}}^+ M_{LO}) \right] d\Phi_2 G_{b/A}(x_1, \mu_f) G_{g/B}(x_2, \mu_f) + [A \leftrightarrow B], \quad (21)$$

where A, B denote the incoming hadrons.

After the renormalization procedure described above, $d\sigma^{Vir}$ is UV-finite. Nevertheless, it contains still the soft and collinear divergences. The soft divergences will cancel against the contributions from real-gluon radiation [see Eq. (24)]. The remaining collinear divergences in the real-gluon-emission processes will be removed by the redefinition of the parton distribution functions (PDF) (mass factorization) [see Eq. (27)].

C. Real corrections

There are three kinds of real corrections to the processes $bg \rightarrow tH^-$: gluon-radiation [$bg \rightarrow tH^-g$], initial-gluon [$gg \rightarrow tH^-\bar{b}$] and initial-active-quark [$bq(\bar{q}) \rightarrow tH^-q(\bar{q})$ and $q\bar{q} \rightarrow tH^-\bar{b}$, where q stand for the active quarks which are treated as light for PDF evolution, in practice the light quarks other than u, d, s can be omitted due to the low luminosity]. All real corrections are related to the $2 \rightarrow 3$ processes.

In this paper, the $2 \rightarrow 3$ processes have been treated using the two cut-off phase space slicing method (TCPSSM) [16]. The method is briefly described in the following. Two small artificial constants δ_s, δ_c are introduced, and the three-body phase space can firstly be divided into soft and hard regions according to whether the gluon energy is less than $\delta_s\sqrt{s}/2$. Secondly the hard region is further divided into hard collinear and hard non-collinear regions according to whether the magnitude of $p_i \cdot p_j$ is less than $\delta_c s/2$ (p_i, p_j are the possible collinear momenta). In the soft and collinear regions, the phase space integration can be performed analytically in $d = 4 - 2\epsilon$ dimensions. At the same time, in the hard non-collinear region, the phase space integration can be calculated in four dimensions by standard Monte Carlo packages because the integration contains no divergences. Obviously, the final physical results should be independent on these artificial parameters δ_s and δ_c , which offers a crucial way to check our results. Therefore, the real corrections can be written technically as, according to the phase space slicing,

$$\sigma^{Real} = \sigma^S + \overline{\sigma^{Coll}} + \sigma^{fin} \quad (22)$$

with

$$\overline{\sigma^{Coll}} = \sigma^{Coll} + \sigma^{fac}, \quad (23)$$

where σ^S , σ^{Coll} and σ^{fin} are cross sections for the direct calculations of the $2 \rightarrow 3$ processes in soft, hard collinear and hard non-collinear regions, and the σ^{fac} is the counter-term from factorization procedure. After adding virtual contributions and σ^S , the double poles are canceled, and the remaining singularities together with σ^{Coll} are canceled by σ^{fac} . In the following, σ^S , $\overline{\sigma^{Coll}}$ and σ^{fin} will be presented respectively.

1. Cross section in soft region

The Feynman diagrams of the gluon-radiation process $bg \rightarrow tH^-g$ are shown in Fig. 3. Diagrams except (c) and (d) contribute to the cross section in the soft region. We may write the cross section as

$$\begin{aligned} \frac{d\sigma^S}{dx_1 dx_2} &= \hat{\sigma}_S^0 G_{b/A}(x_1, \mu_f) G_{g/B}(x_2, \mu_f) + [A \leftrightarrow B], \\ \hat{\sigma}_S^0 &= \hat{\sigma}^0 \left[\frac{\alpha_s}{2\pi} \frac{\Gamma(1-\epsilon)}{\Gamma(1-2\epsilon)} \left(\frac{4\pi\mu^2}{s} \right)^\epsilon \right] \left(\frac{A_2^s}{\epsilon^2} + \frac{A_1^s}{\epsilon} + A_0^s \right), \end{aligned} \quad (24)$$

where

$$\begin{aligned} A_2^s &= -\frac{4}{3} \frac{m_t^2 - t}{(E_1 - \beta \cos \theta)s} + 12 \frac{m_t^2 - u}{(E_1 + \beta \cos \theta)s} + 12, \\ A_1^s &= \frac{16}{3} \frac{4m_t^2}{(E_1^2 - \beta^2)s} + \frac{4}{3} \frac{m_t^2 - t}{(E_1 - \beta \cos \theta)s} (C_1 - 2 \log \frac{2}{\delta_s \sqrt{s}}) \\ &\quad + 12 \frac{m_t^2 - u}{(E_1 + \beta \cos \theta)s} (C_2 - 2 \log \frac{2}{\delta_s \sqrt{s}}) + 24 \log \frac{2}{\delta_s \sqrt{s}} - \log \frac{4}{s} A_2^s, \\ A_0^s &= \frac{1}{2} \log^2 \frac{4}{s} A_2^s - \log \frac{4}{s} A_1^s + \frac{16}{3} \frac{4m_t^2}{(E_1^2 - \beta^2)s} (2 \log \frac{2}{\delta_s \sqrt{s}} + \frac{E_1}{\beta} \log \frac{E_1 + \beta}{E_1 - \beta}) \\ &\quad + \frac{4}{3} \frac{m_t^2 - t}{(E_1 - \beta \cos \theta)s} (C_3 - 2 \log^2 \frac{2}{\delta_s \sqrt{s}} + 2C_1 \log \frac{2}{\delta_s \sqrt{s}}) \\ &\quad - 12 \frac{m_t^2 - u}{(E_1 + \beta \cos \theta)s} (C_4 - 2 \log^2 \frac{2}{\delta_s \sqrt{s}} + 2C_2 \log \frac{2}{\delta_s \sqrt{s}}) + 24 \log^2 \frac{2}{\delta_s \sqrt{s}}, \\ C_1 &= \log \frac{(E_1 - \beta \cos \theta)^2}{E_1^2 - \beta^2}, \\ C_2 &= \log \frac{(E_1 + \beta \cos \theta)^2}{E_1^2 - \beta^2}, \\ C_3 &= -\log^2 \frac{E_1 - \beta}{E_1 - \beta \cos \theta} + \frac{1}{2} \log^2 \frac{E_1 + \beta}{E_1 - \beta} - 2li_2\left(-\frac{-\beta \cos \theta + \beta}{E_1 - \beta}\right) + 2li_2\left(-\frac{\beta \cos \theta + \beta}{E_1 - \beta \cos \theta}\right), \\ C_4 &= -\log^2 \frac{E_1 - \beta}{E_1 + \beta \cos \theta} + \frac{1}{2} \log^2 \frac{E_1 + \beta}{E_1 - \beta} - 2li_2\left(-\frac{\beta \cos \theta + \beta}{E_1 - \beta}\right) + 2li_2\left(-\frac{-\beta \cos \theta + \beta}{E_1 + \beta \cos \theta}\right), \\ \beta &= \lambda^{\frac{1}{2}}(1, m_t^2/s, m_{H^\pm}^2/s), \\ E_1 &= \sqrt{\beta^2 + \frac{2m_t^2}{s}}, \end{aligned} \quad (25)$$

with $\cos \theta$ defined in II-A.

2. Cross section in hard collinear region

As discussed above, the real corrections in collinear region σ^{Coll} contain divergences because the partons are massless. In order to remove these kinds of collinear singularities, we introduce scale dependent parton distribution functions in $\overline{\text{MS}}$ convention

$$G_{c/P}(x, \mu_f) = G_{c/P}(x) - \frac{1}{\epsilon} \left[\frac{\alpha_s}{2\pi} \frac{\Gamma(1-\epsilon)}{\Gamma(1-2\epsilon)} \left(\frac{4\pi\mu^2}{\mu_f^2} \right)^\epsilon \right] \int_x^1 \frac{dz}{z} P_{cc'}(z) G_{c'/P}(x/z), \quad (26)$$

where $P_{cc'}(z)$ are splitting functions and $c[c']$ represent b or g [partons which can split into c]. After substituting the $G_{c/P}(x)$ in the lowest order expressions by $G_{c/P}(x, \mu_f)$, we can obtain σ^{fac} . Adding σ^{Coll} and σ^{fac} , we can get the final results for $\overline{\sigma^{Coll}}$

$$\begin{aligned} \frac{d\overline{\sigma^{Coll}}}{dx_1 dx_2} = & \left[\frac{\alpha_s}{2\pi} \frac{\Gamma(1-\epsilon)}{\Gamma(1-2\epsilon)} \left(\frac{4\pi\mu^2}{s} \right)^\epsilon \right] \left\{ G_{b/A}(x_1, \mu_f) G_{g/B}(x_2, \mu_f) \right. \\ & \times \left[\frac{A_1^{sc}(b \rightarrow bg)}{\epsilon} + \frac{A_1^{sc}(g \rightarrow gg)}{\epsilon} + A_0^{sc}(b \rightarrow bg) + A_0^{sc}(g \rightarrow gg) \right] \\ & + G_{b/A}(x_1, \mu_f) \tilde{G}_{g/B}(x_2, \mu_f) + \tilde{G}_{b/A}(x_1, \mu_f) G_{g/B}(x_2, \mu_f) \Big\} \hat{\sigma}_0 \\ & + [A \leftrightarrow B], \end{aligned} \quad (27)$$

where [16]

$$A_0^{sc} = A_1^{sc} \ln \left(\frac{s}{\mu_f^2} \right) \quad (28)$$

$$A_1^{sc}(b \rightarrow bg) = C_F (2 \ln \delta_s + 3/2) \quad (29)$$

$$A_1^{sc}(g \rightarrow gg) = 2N \ln \delta_s + (11N - 2n_f)/6 \quad (30)$$

with $n_f = 5$ is the number of massless fermions. Here

$$\tilde{G}_{c/B,A}(x, \mu_f) = \sum_{c'} \int_x^{1-\delta_s \delta_{cc'}} \frac{dy}{y} G_{c'/B,A}(x/y, \mu_f) \tilde{P}_{cc'}(y) \quad (31)$$

with

$$\tilde{P}_{ij}(y) = P_{ij}(y) \ln \left(\delta_c \frac{1-y}{y} \frac{s}{\mu_f^2} \right) - P'_{ij}(y), \quad (32)$$

where

$$P_{qq}(z) = C_F \frac{1+z^2}{1-z} \quad (33)$$

$$P'_{qq}(z) = -C_F(1-z) \quad (34)$$

$$P_{gq}(z) = C_F \frac{1 + (1 - z)^2}{z} \quad (35)$$

$$P'_{gq}(z) = -C_F z \quad (36)$$

$$P_{gg}(z) = 2N \left[\frac{z}{1 - z} + \frac{1 - z}{z} + z(1 - z) \right] \quad (37)$$

$$P'_{gg}(z) = 0 \quad (38)$$

$$P_{qg}(z) = \frac{1}{2} [z^2 + (1 - z)^2] \quad (39)$$

$$P'_{qg}(z) = -z(1 - z), \quad (40)$$

with $N = 3$.

3. Cross section in hard non-collinear region

As described above, the cross section in hard non-collinear region σ^{fin} can be easily obtained by Monte Carlo phase space integration in four dimension. It can be written as

$$\frac{d\sigma^{fin}}{dx_1 dx_2} = \sum_{c,c'} G_{c/A}(x_1, \mu_f) G_{c'/B}(x_2, \mu_f) |cc' \rightarrow tH^- X|^2 d\Phi_3 + [A \leftrightarrow B], \quad (41)$$

where c, c' run through gluon and light quarks and the three-body phase space Φ_3 is within the hard non-collinear region. In this paper, all Monte Carlo phase space integrations are performed by package BASES [17].

III. NUMERICAL RESULTS AND DISCUSSION

Our numerical results are obtained using CTEQ5M (CTEQ5L) PDF [18] and 2-loop (1-loop) evolution of $\alpha_s(\mu)$ for NLO (LO) cross section calculations with $\Lambda^{(5)} = 226$ (146) MeV. As we have mentioned in the second section, the dynamical mass of the bottom quark has been set to zero, which means that we treat the bottom quark as usual massless partons. In the \overline{MS} scheme, 2-loop evolution of the quark masses is adopted, and the pole masses of bottom and top quarks are taken as 4.7 GeV and 175 GeV. In the OS scheme (defined in this paper), the top quark mass is equal to the pole mass and the bottom quark mass is the same with that in the \overline{MS} scheme. For simplicity, the renormalization and factorization scales are taken to be the same.

In Fig. 4, we show the cross sections as a function of δ_s with $\delta_c = \delta_s/50$ in the \overline{MS} scheme. It is obviously true that, as stated in II.C, the physical cross sections are independent on the artificial parameters δ_s and δ_c .

A. Theoretical uncertainties

There are many theoretical uncertainties in the calculation of the cross sections, for examples unknown scales of renormalization and factorization as well as the different choice of renormalization schemes. We can define two quantities δ and Δ to measure such kinds of uncertainties as

$$\delta(\mu) = \frac{\sigma_{OS}(\mu) - \sigma_{\overline{MS}}(\mu)}{\sigma_{OS}(\mu) + \sigma_{\overline{MS}}(\mu)}, \quad (42)$$

$$\Delta(\mu) = \frac{\sigma(2\mu) - \sigma(\mu/2)}{\sigma(2\mu) + \sigma(\mu/2)}. \quad (43)$$

It is known that in perturbative calculations, the physical results are independent on the renormalization schemes provided that we can expand the perturbative series to infinity. Otherwise, the results do depend on the renormalization schemes. Therefore δ is due to the unknown parts of higher order effect of the perturbative expansion series, and it can be enhanced by the large term $\log(\mu^2/m_b^2)$, especially for large $\tan\beta$ case, where the yukawa coupling containing m_b dominate the contribution. For such case, δ can be the measure for the entire theoretical uncertainties. Explicitly, for large $\tan\beta$ limit

$$\begin{aligned} \sigma_{LO}^{OS} &\propto m_b^2, \\ \sigma_{LO}^{\overline{MS}} &\propto \overline{m}_b(\mu)^2. \end{aligned} \quad (44)$$

Therefore

$$\delta_{LO} = \frac{m_b^2 - \overline{m}_b(\mu)^2}{m_b^2 + \overline{m}_b(\mu)^2} \simeq \frac{A}{2} \quad (45)$$

with (at one-loop order)

$$A = 2\frac{\alpha_s}{\pi} \left(\log \frac{\mu^2}{m_b^2} + \frac{4}{3} \right), \quad (46)$$

which is the quantity entering also the relation between the \overline{MS} quark mass and the corresponding pole mass,

$$m(\mu)^2 = m^2 [1 - A]. \quad (47)$$

For $\mu = \mu_0 \equiv m_{H^\pm} + m_t$, $\delta_{LO} \simeq 30\%$ if we choose $m_{H^\pm} = 200$ GeV.

At NLO, we can write

$$\begin{aligned} \sigma_{NLO}^{OS} &\propto m_b^2 (1 - A + B), \\ \sigma_{NLO}^{\overline{MS}} &\propto \overline{m}_b(\mu)^2 (1 + B), \end{aligned} \quad (48)$$

where B is the $O(\alpha_s)$ radiative correction to the LO cross section in the \overline{MS} scheme. Hence, one finds

$$\delta_{NLO} \simeq \frac{AB}{2}. \quad (49)$$

For the same μ in the last paragraph, we have $B \simeq 0.3$, and $\delta_{NLO} \simeq 10\%$.

For the small $\tan \beta$ case, where the yukawa coupling containing top quark mass dominates the contribution, δ can be obtained in the similar method as above. For $\mu = \mu_0 = 375$ GeV, $\delta_{LO} \simeq 10\%$ and $\delta_{NLO} \simeq 3\%$. For the intermediate value of $\tan \beta$, δ lies between the large and small $\tan \beta$ case.

From above discussion on δ , we can see that δ at NLO is not large for the small $\tan \beta$ case. Therefore the theoretical uncertainties from varying the renormalization and factorization scales might be more important. In Fig. 5, we show in (a): the LO and NLO cross sections in OS and \overline{MS} schemes and in (b): the relative deviation δ as a function of renormalization and factorization scales μ/μ_0 for $m_{H^\pm} = 200$ GeV and $\tan \beta = 2$. From the figure we can see that the direct calculation confirms the above estimation for δ . Furthermore, the NLO results reduce the scale-dependence in both schemes. From the figure we can also calculate $\Delta_{LO,NLO} \simeq 6\%, 0.2\%$ in OS scheme and $\Delta_{LO,NLO} \simeq 17\%, 5\%$ in \overline{MS} scheme for $\mu = \mu_0$ GeV.

From the discussion on δ and Δ , which act as the measures of the theoretical uncertainties, we can see that the theoretical uncertainties of the cross sections at NLO are much smaller than that at LO.

B. Numerical results in the \overline{MS} scheme

In this section, we will give the numerical results in the \overline{MS} scheme, in which the large terms like $\alpha_s \log(m_b^2/\mu^2)$ have been resummed into the running of the b quark mass.

Therefore it gives usually more stable results with respect to missing higher-order terms.

In Fig. 6 we show the K-factor, which is defined as

$$K = \frac{\sigma_{NLO}}{\sigma_{LO}}, \quad (50)$$

as a function of the charged Higgs mass with the renormalization and factorization scales $\mu = \mu_0$. In the \overline{MS} scheme, if the identical Yukawa couplings are used at LO and NLO calculations, the K-factor does not depend on $\tan\beta$, which is not true in the OS scheme because the different mass renormalization constants of top and bottom quarks spoil it. In Fig. 6, the different contributions to K-factor from improved Born (which is equal to 1 if the difference between the LO and NLO PDF and $\alpha_s(\mu)$ is omitted), virtual+gluon-radiation, initial-gluon, bq (\bar{q}) (q stand for the light quarks) and $q\bar{q}$ are also shown. From the figure, we can see that K-factor from improved Born contribution is around $1.2 \sim 1.3$. K-factor from virtual+gluon-radiation contribution is from 0.7 to 0.9 when the charged Higgs boson mass varies from 200 GeV to 1000 GeV. The initial-gluon and $bq(\bar{q})$ contributions to the K-factor are negative, and they vary from $\sim -27\%$ to $\sim -24\%$ and $\sim -5\%$ to $\sim -14\%$ respectively. The $q\bar{q}$ contribution to the K-factor can be neglected, the magnitude of which is smaller than 3% for all charged Higgs boson mass. Adding all the contributions, we can see that the K-factor varies from ~ 1.6 to ~ 1.8 when charged Higgs mass increases from 200 GeV to 1000 GeV.

In Eq. (50), if we replace the two-loop evolution quark masses by one-loop evolution one in the calculation of the LO cross section, in the \overline{MS} scheme, the K' can be expressed as

$$K' = K \frac{\overline{m}_{t,(2)}^2 + \overline{m}_{b,(2)}^2 \tan^4 \beta}{\overline{m}_{t,(1)}^2 + \overline{m}_{b,(1)}^2 \tan^4 \beta}, \quad (51)$$

where the subscripts of quark masses are which kind of quark mass evolutions are used. In Fig. 7, the K' is shown as a function of charged Higgs boson mass with $\tan\beta = 2, 5, 10, 30$, respectively. The dependence on $\tan\beta$ can be explained by Eq. (51).

To summarize, the next-to-leading order QCD corrections to charged Higgs boson associated production with top quark through $bg \rightarrow tH^-$ at the CERN Large Hadron Collider are calculated in the minimal supersymmetric standard model and two-Higgs-doublet model in the \overline{MS} scheme. It should be noted that in MSSM, the SUSY-QCD corrections arising

from the virtual gluino and squarks should be also included. For some specific parameters, the SUSY-QCD can be significant [7,11]. From the calculations, we can see that the NLO QCD corrections can reduce the scale dependence of the LO cross section. The K-factor does not depend on $\tan\beta$ if the same quark running masses are used in the NLO and LO cross sections, and varies from ~ 1.6 to ~ 1.8 when charged Higgs mass increases from 200 GeV to 1000 GeV.

IV. ACKNOWLEDGEMENT

The author would like to thank Prof. W. Hollik, Prof. C.S. Li, Prof. C.P. Yuan and Dr. J. Guasch for stimulating discussions. This work was supported in part by the Nature Sciences and Engineering Research Council of Canada, the Alexander von Humboldt Foundation and National Nature Science Foundation of China. Parts of the calculations have been performed on the QCM cluster at the University of Karlsruhe, supported by the DFG-Forschergruppe "Quantenfeldtheorie, Computeralgebra und Monte-Carlo-Simulation".

[1] For example to see, L. G. Jin, C. S. Li, R. J. Oakes and S. H. Zhu, Phys. Rev. D **62**, 053008 (2000) [arXiv:hep-ph/0003159], and references therein.

[2] W. Hollik and S. h. Zhu, Phys. Rev. D **65**, 075015 (2002) [arXiv:hep-ph/0109103].

[3] D. P. Roy, Phys. Lett. B **459**, 607 (1999) [arXiv:hep-ph/9905542].

[4] K. Odagiri, arXiv:hep-ph/9901432; K. Odagiri, Phys. Lett. B **452**, 327 (1999) [arXiv:hep-ph/9902303].

[5] J. C. Collins and W. K. Tung, Nucl. Phys. B **278**, 934 (1986); F. I. Olness and W. K. Tung, Nucl. Phys. B **308**, 813 (1988); R. M. Barnett, H. E. Haber and D. E. Soper, Nucl. Phys. B **306**, 697 (1988).

[6] See for example, M. Spira, talk given at 10th International Conference on Supersymmetry and Unification of Fundamental Interactions, June 17-23, 2002, DESY Hamburg, <http://www.desy.de/~susy02/pl.1c/spira.pdf>.

[7] T. Plehn, hep-ph/0206121.

[8] F. Borzumati, J. L. Kneur and N. Polonsky, Phys. Rev. D **60**, 115011 (1999) [arXiv:hep-ph/9905443].

[9] L. G. Jin, C. S. Li, R. J. Oakes and S. H. Zhu, Eur. Phys. J. C **14**, 91 (2000) [arXiv:hep-ph/9907482].

[10] A. Belyaev, D. Garcia, J. Guasch and J. Sola, arXiv:hep-ph/0105053; C. S. Huang and S. H. Zhu, Phys. Rev. D **60**, 075012 (1999) [arXiv:hep-ph/9812201].

[11] G. p. Gao, G. r. Lu, Z. h. Xiong and J. M. Yang, arXiv:hep-ph/0202016.

[12] J. Campbell, R. K. Ellis, F. Maltoni and S. Willenbrock, arXiv:hep-ph/0204093.

[13] J. Küblbeck, M. Böhm and A. Denner, *Comput. Phys. Commun.* **60**, 165 (1990); T. Hahn, [hep-ph/9905354](#).

[14] R. Mertig, M. Böhm and A. Denner, *Comput. Phys. Commun.* **64**, 345 (1991).

[15] W. Beenakker, R. Hopker, M. Spira and P. M. Zerwas, *Nucl. Phys. B* **492**, 51 (1997) [[arXiv:hep-ph/9610490](#)].

[16] For example to see, B. W. Harris and J. F. Owens, *Phys. Rev. D* **65**, 094032 (2002) [[arXiv:hep-ph/0102128](#)].

[17] S. Kawabata, *Comput. Phys. Commun.* 88, 309 (1995).

[18] H. L. Lai *et al.* [CTEQ Collaboration], *Eur. Phys. J. C* **12**, 375 (2000) [[hep-ph/9903282](#)].

[19] G. J. van Oldenborgh and J. A. Vermaseren, *Z. Phys. C* **46**, 425 (1990).

V. APPENDIX

In this appendix, we will give the non-vanishing form-factors in Eq. (16). For completeness, we give firstly the definition of loop integrals and its Lorentz decomposition:

$$B_0(p_1^2, m_0^2, m_1^2) = \frac{(2\pi\mu)^{4-d}}{i\pi^2} \int d^d q \frac{1}{Q_0 Q_1}, \quad (52)$$

$$C_{0;\mu;\mu\nu}(p_1^2, p_{12}, p_2^2, m_0^2, m_1^2, m_2^2) = \frac{(2\pi\mu)^{4-d}}{i\pi^2} \int d^d q \frac{1; q_\mu; q_\mu q_\nu}{Q_0 Q_1 Q_2}, \quad (53)$$

$$D_{0;\mu;\mu\nu}(p_1^2, p_{12}, p_{32}, p_3^2, p_2^2, p_{31}, m_0^2, m_1^2, m_2^2, m_3^2) = \frac{(2\pi\mu)^{4-d}}{i\pi^2} \int d^d q \frac{1; q_\mu; q_\mu q_\nu}{Q_0 Q_1 Q_2 Q_3} \quad (54)$$

with

$$Q_0 = q^2 - m_0^2 + i\epsilon, \quad Q_i = (q + p_i)^2 - m_i^2 + i\epsilon, \quad p_{ij} = (p_i - p_j)^2 \quad (55)$$

and

$$\begin{aligned}
C_\mu &= p_{1\mu}C_1 + p_{2\mu}C_2 \\
C_{\mu\nu} &= g_{\mu\nu}C_{00} + p_{1\mu}p_{1\nu}C_{11} + (p_{1\mu}p_{2\nu} + p_{2\mu}p_{1\nu})C_{12} + p_{2\mu}p_{2\nu}C_{22} \\
D_\mu &= p_{1\mu}D_1 + p_{2\mu}D_2 + p_{3\mu}D_3 \\
D_{\mu\nu} &= g_{\mu\nu}D_{00} + p_{1\mu}p_{1\nu}D_{11} + (p_{1\mu}p_{2\nu} + p_{2\mu}p_{1\nu})D_{12} + (p_{1\mu}p_{3\nu} + p_{3\mu}p_{1\nu})D_{13} \\
&\quad + p_{2\mu}p_{2\nu}D_{22} + (p_{2\mu}p_{3\nu} + p_{3\mu}p_{2\nu})D_{23} + p_{3\mu}p_{3\nu}D_{33}.
\end{aligned} \tag{56}$$

For simplicity, we define abbreviation for $B_0^i (i = 1 - 7)$, $C_x^i (i = 1 - 8)$ [x stands for the subscript defined in Eq. (56)], $D_0^i (i = 1 - 3)$ as

$$\begin{aligned}
B_0^1 &= B_0(0, 0, m_t^2), \\
B_0^2 &= B_0(0, m_t^2, m_t^2), \\
B_0^3 &= B_0(m_{H^\pm}^2, 0, m_t^2), \\
B_0^4 &= B_0(m_t^2, 0, m_t^2), \\
B_0^5 &= B_0(s, 0, 0), \\
B_0^6 &= B_0(t, 0, m_t^2), \\
B_0^7 &= B_0(u, 0, m_t^2), \\
C_x^1 &= C_x(0, 0, s, 0, 0, 0), \\
C_x^2 &= C_x(0, m_{H^\pm}^2, t, m_t^2, m_t^2, 0), \\
C_x^3 &= C_x(m_{H^\pm}^2, 0, t, m_t^2, 0, 0), \\
C_x^4 &= C_x(m_{H^\pm}^2, 0, u, m_t^2, 0, 0), \\
C_x^5 &= C_x(m_{H^\pm}^2, m_t^2, s, 0, m_t^2, 0), \\
C_x^6 &= C_x(m_t^2, 0, t, m_t^2, 0, 0), \\
C_x^7 &= C_x(m_t^2, 0, u, 0, m_t^2, m_t^2), \\
C_x^8 &= C_x(m_t^2, 0, u, m_t^2, 0, 0), \\
D_0^1 &= D_0(m_{H^\pm}^2, 0, m_t^2, 0, t, u, 0, m_t^2, m_t^2, 0), \\
D_0^2 &= D_0(m_{H^\pm}^2, m_t^2, 0, 0, s, t, 0, m_t^2, 0, 0), \\
D_0^3 &= D_0(m_{H^\pm}^2, m_t^2, 0, 0, s, u, 0, m_t^2, 0, 0).
\end{aligned} \tag{57}$$

For diagram (e) in Fig. 2, we can write the form factor as

$$f_i = \frac{C_A}{2} \frac{g_s^3}{16\pi^2 s} g_i \quad (58)$$

$$\begin{aligned} g_2 &= -2B_0^5 - s[C_0^1 + 3(C_1^1 + C_2^1)] + 4(-1 + 2\epsilon)C_{00}^1, \\ g_5 &= 2[B_0^5(1 + \epsilon) + s(C_0^1 + 2C_1^1 - 3C_2^1)]. \end{aligned} \quad (59)$$

For diagram (f) in Fig. 2, we can write the form factor as

$$f_i = (C_F - C_A/2) \frac{g_s^3}{8\pi^2 s} g_i \quad (60)$$

$$\begin{aligned} g_2 &= -B_0^5 - (1 + \epsilon)s(C_0^1 + C_1^1 + C_2^1) + 2(1 - \epsilon)C_{00}^1, \\ g_5 &= (1 + \epsilon)B_0^5 + 2\epsilon sC_1^1 - 2(1 + \epsilon)sC_2^1. \end{aligned} \quad (61)$$

For diagram (g) in Fig. 2, we can write the form factor as

$$f_i = C_F \frac{g_s^3}{8\pi^2 s} g_i \quad (62)$$

$$\begin{aligned} g_1 &= m_t s(C_0^5(1 - \epsilon) + C_2^5 - \epsilon(C_1^5 + C_2^5)), \\ g_2 &= \frac{g_5}{2} = C_0^5(m_{H^\pm}^2 - 2m_t^2) - B_0^4 - B_0^5 - m_t^2(C_1^5 + C_2^5) + \epsilon(B_0^3 + sC_2^5). \end{aligned} \quad (63)$$

For diagram (h) in Fig. 2, we can write the form factor as

$$f_i = C_F \frac{g_s^3}{8\pi^2(m_t^2 - u)} g_i \quad (64)$$

$$\begin{aligned} g_1 &= m_t(-1 + \epsilon)(m_t^2 - u)(C_0^4 + C_1^4 + C_2^4), \\ g_2 &= \frac{g_3}{2} = -C_0^4[m_{H^\pm}^2 + (-2 + \epsilon)m_t^2 - \epsilon u] + B_0^7 \\ &\quad + m_t^2(C_1^4 + C_2^4) - \epsilon[B_0^3 + (m_t^2 - u)(C_1^4 + C_2^4)]. \end{aligned} \quad (65)$$

For diagram (i) in Fig. 2, we can write the form factor as

$$f_i = \frac{C_A}{2} \frac{g_s^3}{16\pi^2(m_t^2 - u)} g_i \quad (66)$$

$$\begin{aligned} g_1 &= 3m_t(m_t^2 - u)C_2^8, \\ g_2 &= 2B_0^4 + 2B_0^7 + (m_t^2 - u)(2C_0^8 + 3C_1^8) + 4(1 - \epsilon)C_{00}^8, \\ g_3 &= 2\{\epsilon - 1 + C_0^8(m_t^2 - u) - (1 + \epsilon)B_0^4 + 2B_0^7 + m_t^2[-5C_1^8 + 4C_2^8 + 2(1 - \epsilon)C_{11}^8] \\ &\quad + u[C_1^8 - 4C_2^8 - 2(1 - \epsilon)C_{11}^8]\}, \\ g_4 &= 4m_t[C_1^8 - 2C_2^8 - (1 - \epsilon)C_{11}^8]. \end{aligned} \quad (67)$$

For diagram (j) in Fig. 2, we can write the form factor as

$$f_i = (C_F - C_A/2) \frac{g_s^3}{8\pi^2(m_t^2 - u)} g_i \quad (68)$$

$$\begin{aligned} g_1 &= m_t(m_t^2 - u)[C_2^7 + \epsilon(C_0^7 + C_2^7)], \\ g_2 &= 2C_0^7 m_t^2 - (1 + \epsilon)B_0^2 + B_0^4 + B_0^7 + (1 + \epsilon)(m_t^2 - u)C_1^7 + 2(-1 + \epsilon)C_{00}^7, \\ g_3 &= -1 - B_0^4 + 2B_0^7 + 2uC_{22}^7 - 2m_t^2(2C_2^7 + C_{22}^7) \\ &\quad - \epsilon[-1 + B_0^4 - 2(m_t^2 - u)(C_2^7 + C_{22}^7)], \\ g_4 &= -2m_t[C_0^7 \epsilon + (-1 + 2\epsilon)C_2^7 + (-1 + \epsilon)C_{22}^7]. \end{aligned} \quad (69)$$

For diagram (k) in Fig. 2, we can write the form factor as

$$f_i = C_F \frac{g_s^3}{16\pi^2 s} g_i \quad (70)$$

$$g_2 = \frac{g_5}{2} = (1 - \epsilon)B_0^5. \quad (71)$$

For diagram (l) in Fig. 2, we can write the form factor as

$$f_i = C_F \frac{g_s^3}{16\pi^2(m_t^2 - u)^2 u} g_i \quad (72)$$

$$\begin{aligned} g_1 &= -m_t(m_t^2 - u) \left\{ (\epsilon - 1)m_t^2(B_0^1 - B_0^7) + u(\epsilon - 3)B_0^7 \right\}, \\ g_2 &= \frac{g_3}{2} = (-1 + \epsilon)m_t^4(B_0^1 - B_0^7) - (-1 + \epsilon)u^2 B_0^7 \\ &\quad + m_t^2 u \left\{ (1 - \epsilon)[B_0^1 - 2(1 + B_0^2)] + 2(-3 + \epsilon)B_0^7 \right\}. \end{aligned} \quad (73)$$

For diagram (m) in Fig. 2, we can write the form factor as

$$f_i = \frac{C_A}{2} \frac{g_s^3}{16\pi^2} g_i \quad (74)$$

$$\begin{aligned} g_1 &= -m_t[C_0^8 + C_1^8 + C_2^8 - 2(s - u + m_t^2)(D_0^3 + D_1 + D_2 + D_3) + 4D_{00}], \\ g_2 &= -2(C_0^4 + C_0^5) - 2D_0^3(m_t^2 - u) + C_1^1 + C_1^8 + 2(t + 2u)(D_2 + D_3) \\ &\quad - m_{H^\pm}^2(D_1 + 2D_2 + D_3) - m_t^2(D_1 + 4D_2 + 3D_3) + 4\epsilon D_{00}, \\ g_3 &= -2 \left\{ 2[C_0^4 - (1 + \epsilon)C_0^5 + C_0^8] - 2\epsilon(C_1^5 + C_2^5) + C_1^8 + C_2^8 + 2D_0^3[-m_{H^\pm}^2 + (1 - \epsilon)m_t^2] \right. \\ &\quad \left. - 2m_t^2(D_1 + 2D_2 + D_3) - m_t^4(D_1 + 4D_2 + 3D_3) + 4\epsilon D_{00} \right\}. \end{aligned}$$

$$\begin{aligned}
& + (1 + \epsilon)u] + 2[(3 - 2\epsilon)m_t^2 - t + 2u\epsilon](D_1 + D_2 + D_3) + 2[(1 - \epsilon)m_t^2 + u\epsilon](D_{11} \\
& + 2D_{12} + 2D_{13} + D_{22} + 2D_{23} + D_{33})\} , \\
g_4 & = 4m_t \left\{ (D_2 + D_3 + D_{11} + 2D_{12} + D_{13} + D_{22} + D_{23}) - \epsilon[D_0^3 + D_{11} + D_{22} + D_{33} \right. \\
& \left. + 2(D_1 + D_2 + D_3 + D_{12} + D_{13} + D_{23})]\} , \\
g_5 & = 4m_t \left\{ C_0^1 + 2\epsilon C_1^5 - C_1^1 + 2(u - m_t^2)D_1 + [m_{H^\pm}^2 - (7 - 2\epsilon)m_t^2 + 2(t + 2u) - 2u\epsilon]D_2 \right. \\
& \left. + [-m_{H^\pm}^2 - m_t^2 + 2s]D_3 + [2(\epsilon - 1)m_t^2 - 2u\epsilon](D_{12} + D_{22} + D_{23})\right\} , \\
g_6 & = -4m_t[D_0^3 + D_1 + (2 - \epsilon)D_2 + D_3 + D_{12} + D_{22}] , \tag{75}
\end{aligned}$$

where the variable of the D-function is the same with D_0^3 .

For diagram (n) in Fig. 2, we can write the form factor as

$$f_i = (C_F - C_A/2) \frac{g_s^3}{8\pi^2} g_i \tag{76}$$

$$\begin{aligned}
g_1 & = -m_t \left\{ D_0^1[s + \epsilon(m_t^2 - u)] + s(D_2 + D_3) \right. \\
& \left. - \epsilon[C_2^6 - m_t^2(D_1 + D_3) + u(D_2 + D_3)] - 2D_{00}\right\} , \\
g_2 & = -C_0^4 - C_0^7 + C_0^2(2 + \epsilon) + D_0^1[m_{H^\pm}^2 + \epsilon m_t^2 - (2 + \epsilon)u] + D_1[m_t^2(1 + \epsilon) \\
& + s - u(1 + \epsilon)] + (D_2 + D_3)[\epsilon m_t^2 + s - u(1 + \epsilon)] - 2\epsilon D_{00} , \\
g_3 & = 2 \left\{ -C_0^4 - C_0^7 - (C_1^7 + C_2^7) - \epsilon(C_1^2 + C_2^6) + 2m_t^2 D_2 - t(D_2 + D_3) + m_t^2(2D_3 + D_{22} \right. \\
& \left. + 2D_{23} + D_{33}) - \epsilon \left[C_2 + (m_t^2 - u)[D_2 + D_3 + D_{22} + 2D_{23} + D_{33}]\right] \right\} , \\
g_4 & = 2m_t \left\{ -D_2 - D_3 - D_{12} - D_{13} - D_{22} - 2D_{23} - D_{33} \right. \\
& \left. + \epsilon[D_0^1 + 2D_2 + 2D_3 + D_{22} + 2D_{23} + D_{33}]\right\} , \\
g_5 & = -2 \left\{ C_0^6(-1 + \epsilon) + (4m_t^2 - t - 2u)D_2 - sD_3 + m_t^2(D_{22} + D_{23}) \right. \\
& \left. + \epsilon[2C_1^6 - C_1^2 + C_2^6 - (m_t^2 - u)(D_3 + D_{22} + D_{23})]\right\} , \\
g_6 & = 2m_t[D_0 - (-3 + \epsilon)D_2 + D_{12} - (-1 + \epsilon)(D_{22} + D_{23})] , \tag{77}
\end{aligned}$$

where the variable of the D-function is the same with D_0^1 .

For diagram (o) in Fig. 2, we can write the form factor as

$$f_i = (C_F - C_A/2) \frac{g_s^3}{8\pi^2} g_i \tag{78}$$

$$g_1 = -m_t[C_0^5 - \epsilon C_0^6 + D_0^2(1 + \epsilon)s - \epsilon(C_1^6 + C_2^6) + s(1 + \epsilon)(D_1 + D_2 + D_3) - 2D_{00}] ,$$

$$\begin{aligned}
g_2 &= -C_0^1 - C_0^5 + C_0^3(2 + \epsilon) + D_0^2(-2m_t^2 + t) - m_t^2(D_1 + D_2) \\
&\quad + [s(1 + \epsilon) - u]D_3 - 2\epsilon D_{00}, \\
g_3 &= 2 \left\{ C_0^5(1 + \epsilon) - C_0^6\epsilon + D_0^2[2m_{H^\pm}^2 + m_t^2(4 - \epsilon) - s(2 - \epsilon) - 3t - u(2 - \epsilon)] \right. \\
&\quad \left. + \epsilon(C_1^3 + C_1^5 - C_1^6 + C_2^5 - C_2^6) + (D_1 + D_2 + D_3)[m_{H^\pm}^2(-3 + \epsilon) - m_t^2\epsilon + 3s + t(2 - \epsilon)] \right. \\
&\quad \left. + u(3 + \epsilon)] + (D_{11} + 2D_{12} + 2D_{13} + D_{22} + 2D_{23} + D_{33})[m_t^2(1 - \epsilon) + \epsilon u] \right\}, \\
g_4 &= 2m_t \left\{ -D_3 - D_{13} - D_{23} - D_{33} + \epsilon(D_0 + 2D_1 + 2D_2 + 2D_3 + D_{11} \right. \\
&\quad \left. + 2D_{12} + 2D_{13} + D_{22} + 2D_{23} + D_{33}) \right\}, \\
g_5 &= -2 \left\{ C_0^6 - D_0^2(m_{H^\pm}^2 - 2m_t^2) - C_1^1 + \epsilon(C_1^3 + C_2^5) + D_1[-t(1 + \epsilon) - 2u] + \right. \\
&\quad (D_2 + D_3)[\epsilon m_{H^\pm}^2 - s(1 + \epsilon)] + D_3[-t(1 + \epsilon) - u] + (D_{11} + D_{12} + 2D_{13} + D_{23} + D_{33})u\epsilon \\
&\quad \left. + m_t^2[5D_1 + D_2 + 4D_3 - (-1 + \epsilon)(D_{11} + D_{12} + 2D_{13} + D_{23} + D_{33})] \right\}, \\
g_6 &= 2m_t \left\{ D_0^2 - (-2 + \epsilon)(D_1 + D_3) + D_{13} + D_{33} - \epsilon(D_{11} + D_{12} + 2D_{13} + D_{23} + D_{33}) \right\}, \quad (79)
\end{aligned}$$

where the variable of the D-function is the same with D_0^2 .

By decomposition, the loop integrals in above form-factors can be calculated by the limit number of scalar integrals B_0, C_0 and D_0 . The scalar integrals C_0 and D_0 are UV finite, however some of them contain soft and collinear divergences. Because the finite scalar integrals could be calculated by numerical method [19], only the divergent ones are presented explicitly in this paper. It should be noted that only real part of the integrals, which is relevant to our results, is given.

D_0 and C_0 scalar integrates could be generally written as

$$\begin{aligned}
D_0 &= (4\pi\mu^2)^\epsilon \Gamma(1 + \epsilon) \left(\frac{d_2}{\epsilon^2} + \frac{d_1}{\epsilon} + d_0 \right), \\
C_0 &= -(4\pi\mu^2)^\epsilon \Gamma(1 + \epsilon) \left(\frac{c_2}{\epsilon^2} + \frac{c_1}{\epsilon} + c_0 \right). \quad (80)
\end{aligned}$$

The coefficients d_2, d_1 and d_0 of D_0^1 are

$$d_2 = \frac{1}{2(m_t^2 - t)(m_t^2 - u)}, \quad (81)$$

$$d_1 = \frac{1}{(m_t^2 - t)(m_t^2 - u)} \log \frac{m_t(m_t^2 - m_{H^\pm}^2)}{(m_t^2 - t)(m_t^2 - u)}, \quad (82)$$

$$d_0 = \frac{1}{2(m_t^2 - t)(m_t^2 - u)} \left\{ \pi^2 \left[\theta(m_{H^\pm} - m_t) - \frac{1}{3} \right] - 2\log^2 m_t + 3\log^2(m_t^2 - t) \right\}$$

$$\begin{aligned}
& +3 \log ^2\left(m_t^2-u\right)-2 \log \left(m_t^2-t\right) \log (t)-2 \log \left(m_t^2-u\right) \log (u)-3 \log ^2\left|m_{H^{\pm}}^2-m_t^2\right| \\
& +4 \log \left(m_{H^{\pm}}\right) \log \frac{m_{H^{\pm}}^2-m_t^2}{m_t^2}-4 \log \left(m_t\right) \log \frac{\left(m_t^2-t\right) \left(m_t^2-u\right)}{t u \left(m_{H^{\pm}}^2-m_t^2\right)}-2 l i_2\left(\frac{m_{H^{\pm}}^2 s}{\left(m_{H^{\pm}}^2-t\right) \left(m_{H^{\pm}}^2-u\right)}\right) \\
& -2 l i_2\left(\frac{\left(m_t^2-t\right) u}{m_t^2 \left(u-m_{H^{\pm}}^2\right)}\right)-2 l i_2\left(\frac{m_t^2}{m_t^2-m_{H^{\pm}}^2}\right)+2 l i_2\left(\frac{u-m_{H^{\pm}}^2}{m_t^2-t}\right)+2 l i_2\left(\frac{m_t^2}{m_t^2-t}\right) \\
& +2 l i_2\left(\frac{t-m_{H^{\pm}}^2}{m_t^2-u}\right)-2 l i_2\left(\frac{\left(t-m_{H^{\pm}}^2\right) \left(u-m_{H^{\pm}}^2\right)}{\left(m_t^2-t\right) \left(m_t^2-u\right)}\right)+2 l i_2\left(\frac{m_t^2}{m_t^2-u}\right)-2 l i_2\left(\frac{t \left(u-m_t^2\right)}{m_t^2 \left(m_{H^{\pm}}^2-t\right)}\right) \\
& +2 l i_2\left(\frac{m_{H^{\pm}}^2 \left(m_t^2-t\right) \left(m_t^2-u\right)}{m_t^2 \left(m_{H^{\pm}}^2-u\right) \left(m_{H^{\pm}}^2-t\right)}\right)+2 l i_2\left(\frac{t s}{\left(m_{H^{\pm}}^2-t\right) \left(t-m_t^2\right)}\right) \\
& -2 l i_2\left(\frac{m_t^2 s}{\left(m_t^2-t\right) \left(m_t^2-u\right)}\right)+2 l i_2\left(\frac{s u}{\left(m_{H^{\pm}}^2-u\right) \left(u-m_t^2\right)}\right)\Big\}. \tag{83}
\end{aligned}$$

The coefficients d_2 , d_1 and d_0 of D_0^2 are

$$d_2 = \frac{3}{2 s \left(t-m_t^2\right)}, \tag{84}$$

$$d_1 = \frac{1}{s \left(t-m_t^2\right)} \log \frac{m_t \left(m_{H^{\pm}}^2-m_t^2\right)}{s \left(m_t^2-t\right)^2}, \tag{85}$$

$$\begin{aligned}
d_0 = & \frac{1}{2 s \left(m_t^2-t\right)} \left\{ \pi^2 \left[1-\theta\left(m_{H^{\pm}}-m_t\right)\right]+2 \log ^2\left(m_t\right)+\log ^2\left|m_{H^{\pm}}^2-m_t^2\right|-\log ^2\left(m_t^2-t\right) \right. \\
& -2 \log \left(m_{H^{\pm}}^2-t\right) \log \left(m_t^2-t\right)+4 \log \frac{s}{m_{H^{\pm}}^2-t} \log \frac{m_t}{m_t^2-t}-2 l i_2\left(\frac{m_{H^{\pm}}^2}{m_{H^{\pm}}^2-m_t^2}\right) \\
& \left. +2 l i_2\left(\frac{m_t^2-t}{m_t^2}\right)-2 l i_2\left(\frac{m_{H^{\pm}}^2 \left(m_t^2-t\right)}{m_t^2 \left(m_{H^{\pm}}^2-t\right)}\right)+2 l i_2\left(\frac{m_{H^{\pm}}^2}{m_{H^{\pm}}^2-t}\right)+2 l i_2\left(\frac{m_{H^{\pm}}^2-t}{m_t^2-t}\right)\right\}. \tag{86}
\end{aligned}$$

The coefficients c_2 , c_1 and c_0 of C_0^1 are

$$c_2 = -\frac{1}{s}, \tag{87}$$

$$c_1 = \frac{\log (s)}{s}, \tag{88}$$

$$c_0 = \frac{1}{6 s} \left[4 \pi^2-3 \log ^2(s)\right]. \tag{89}$$

The coefficients c_1 and c_0 of C_0^3 are

$$c_1 = \frac{1}{m_{H^{\pm}}^2-t} \log \left(\frac{m_t^2-m_{H^{\pm}}^2}{m_t^2-t}\right), \tag{90}$$

$$c_0 = \frac{1}{2(m_{H^\pm}^2 - t)} \left\{ \log^2(m_t^2 - t) - \log^2(m_t^2 - m_{H^\pm}^2) + 2li_2\left(\frac{m_{H^\pm}^2}{m_{H^\pm}^2 - m_t^2}\right) - 2li_2\left(\frac{t}{t - m_t^2}\right) \right\}. \quad (91)$$

The coefficients c_2, c_1 and c_0 of C_0^6 are

$$c_2 = \frac{1}{2(m_t^2 - t)}, \quad (92)$$

$$c_1 = \frac{1}{(m_t^2 - t)} \log \frac{m_t}{m_t^2 - t}, \quad (93)$$

$$c_0 = \frac{1}{2(m_t^2 - t)} \left\{ -\log(m_t) + \log^2(m_t^2 - t) - 2li_2\left(\frac{t}{t - m_t^2}\right) \right\}. \quad (94)$$

C_0^4 , C_0^8 and D_0^3 can be obtained from C_0^3 , C_0^6 and D_0^2 by replacing t with u .

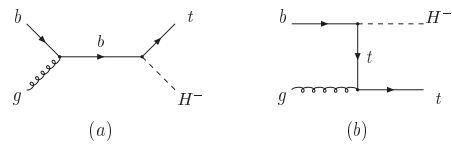


FIG. 1. Feynman diagrams at LO for $bg \rightarrow tH^-$.

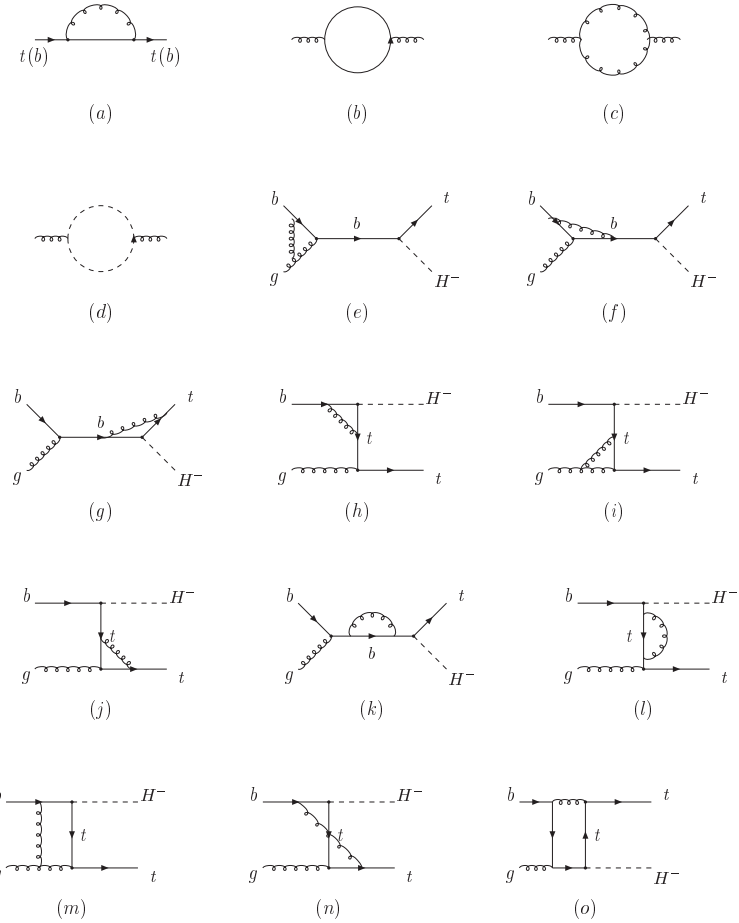


FIG. 2. Feynman diagrams of the virtual correction for the process $bg \rightarrow tH^-$.

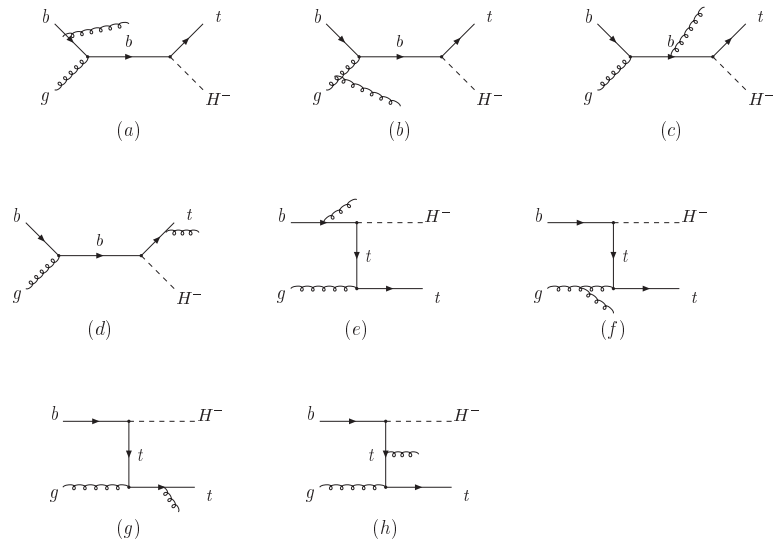


FIG. 3. Feynman diagrams of gluon-radiation process of $bg \rightarrow tH^- g$.

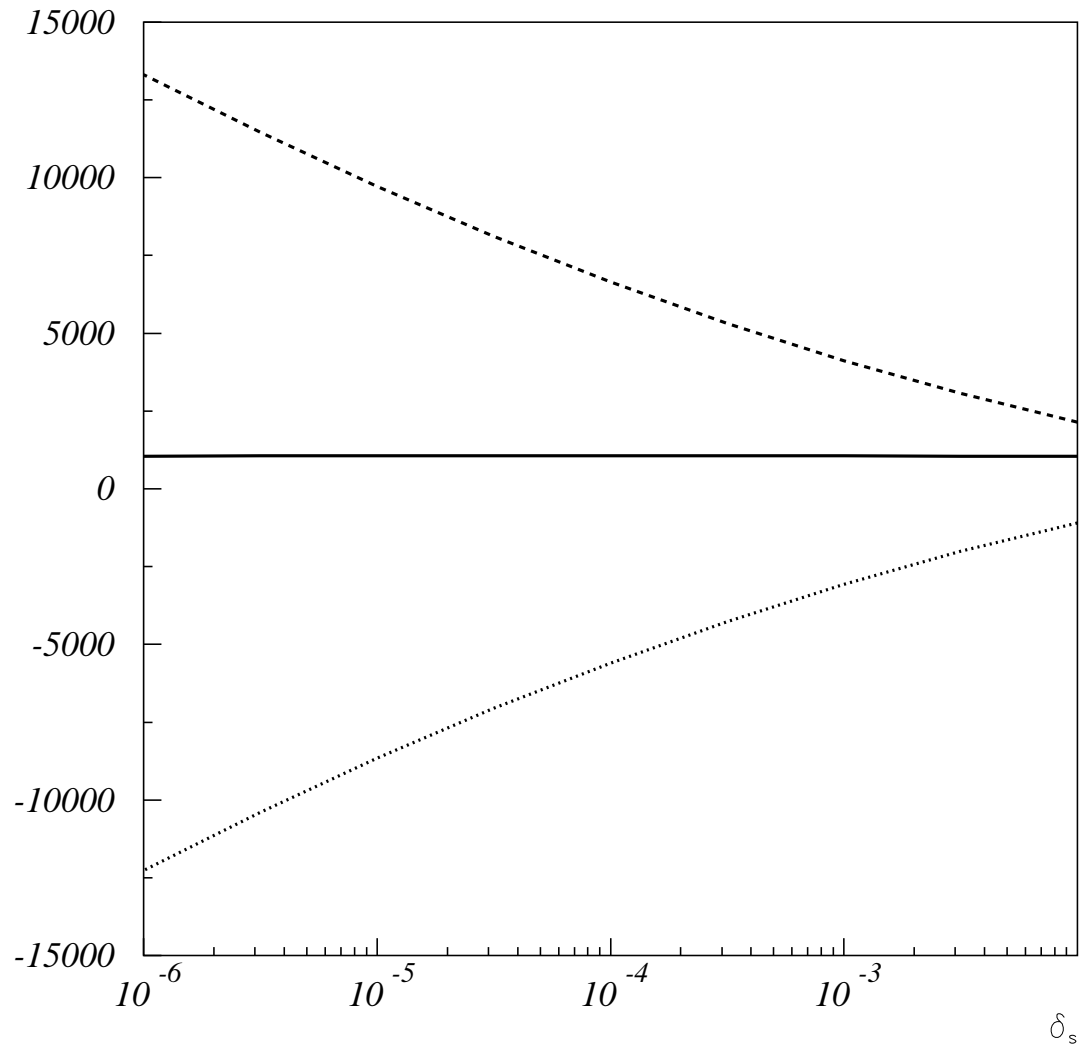


FIG. 4. The cross sections [in fb] from hard non-collinear regions (dashed), other than hard non-collinear regions (dotted) and total (solid) as a function of δ_s with $\delta_c = \delta_s/50$, where $\tan \beta = 2$, $m_{H^\pm} = 200$ GeV and renormalization and factorization scales $\mu = m_{H^\pm} + m_t$.

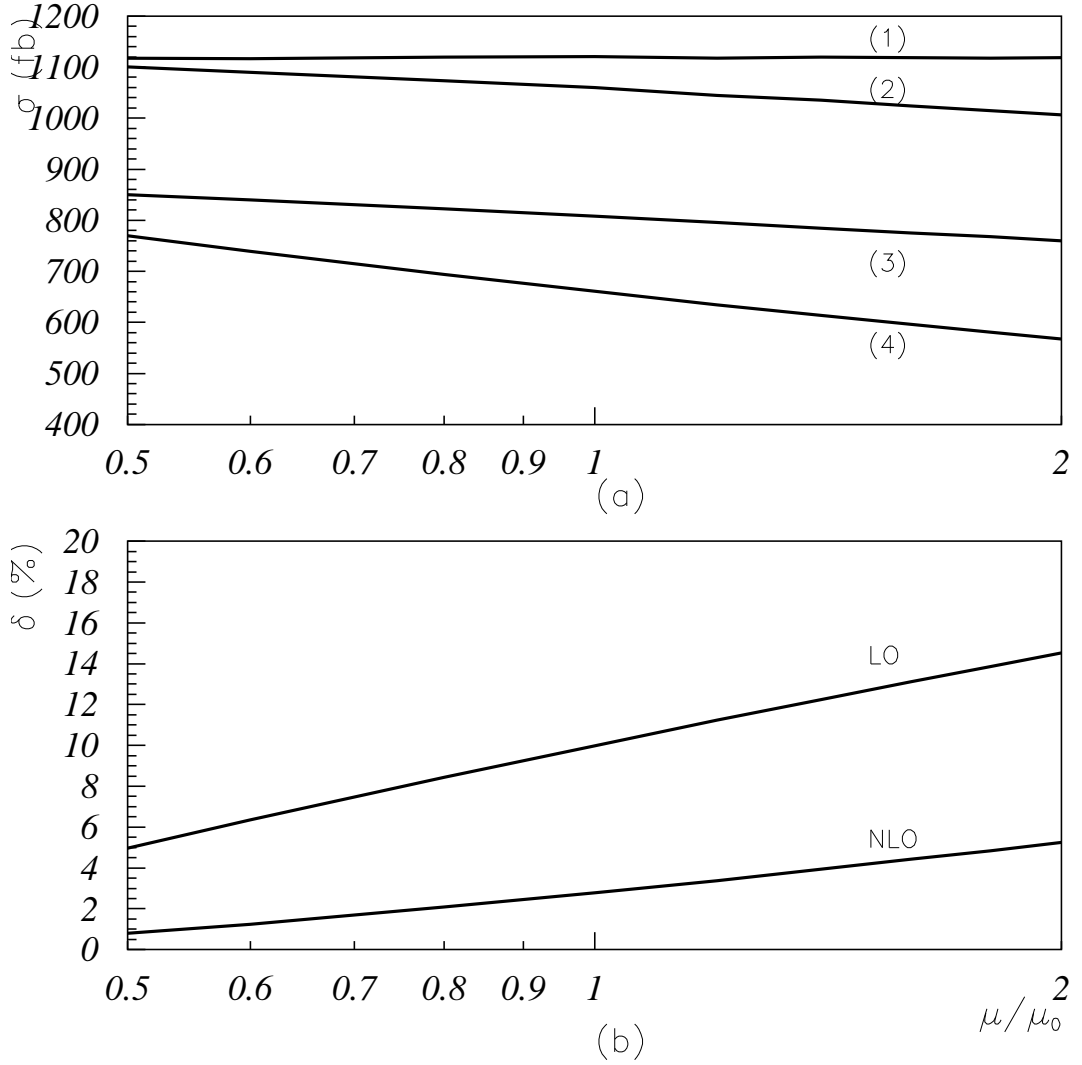


FIG. 5. (a): the total cross sections as a function of μ/μ_0 with $\mu_0 = m_{H^\pm} + m_t$, where $\tan \beta = 2$ and $m_{H^\pm} = 200$ GeV. Curves (1)-(4) represent the cross section at NLO in OS scheme (1), NLO in \overline{MS} scheme (2), LO in OS scheme (3), LO in \overline{MS} scheme (4). (b): δ (defined in text) as a function of μ/μ_0 .

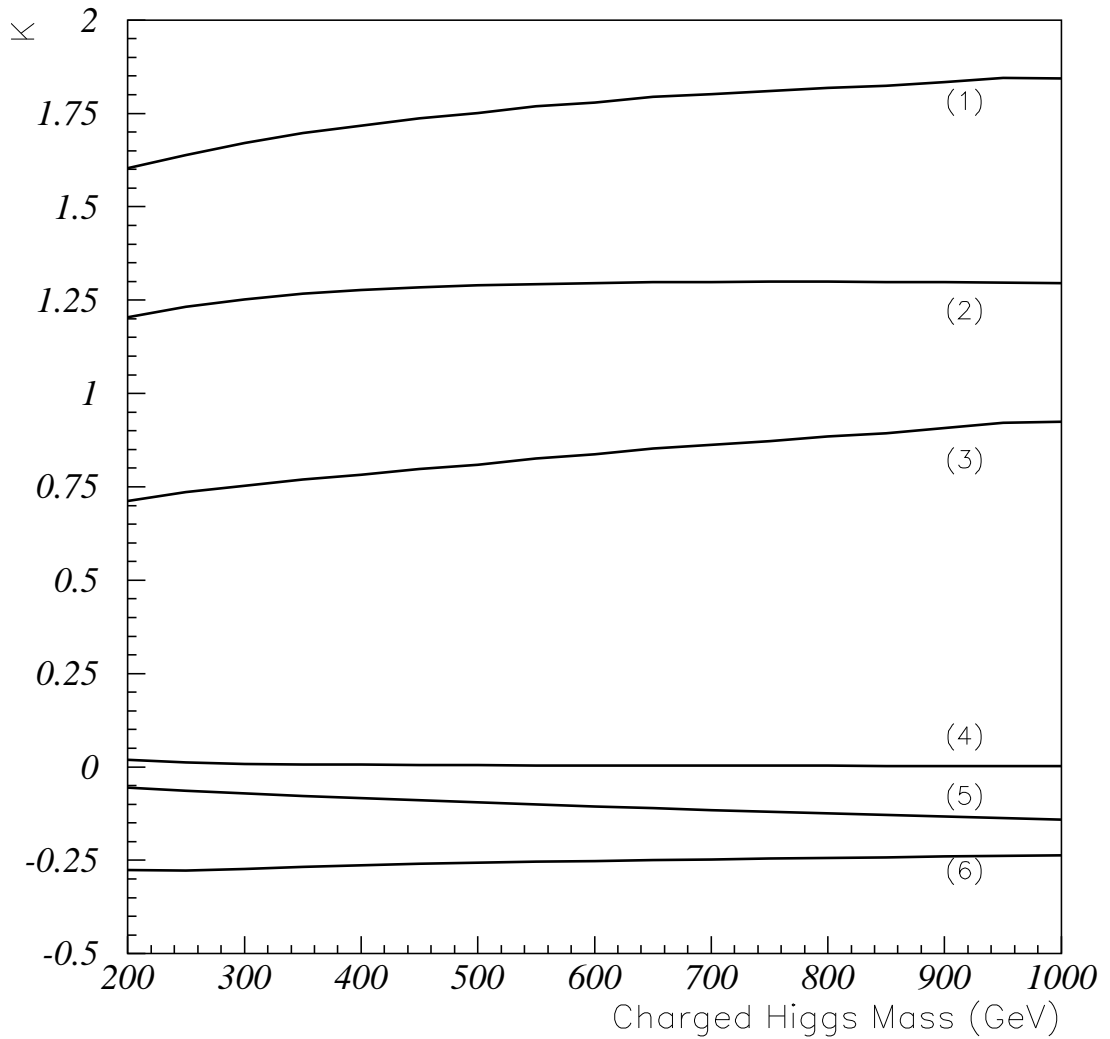


FIG. 6. Various contributions to K-factor versus m_{H^\pm} with $\mu = \mu_0$. Curves (1)-(6) represent contributions from all (1), improved Born (2), virtual plus gluon-radiation (3), $q\bar{q}$ (4), $bq(\bar{q})$ (5) and initial-gluon (6).

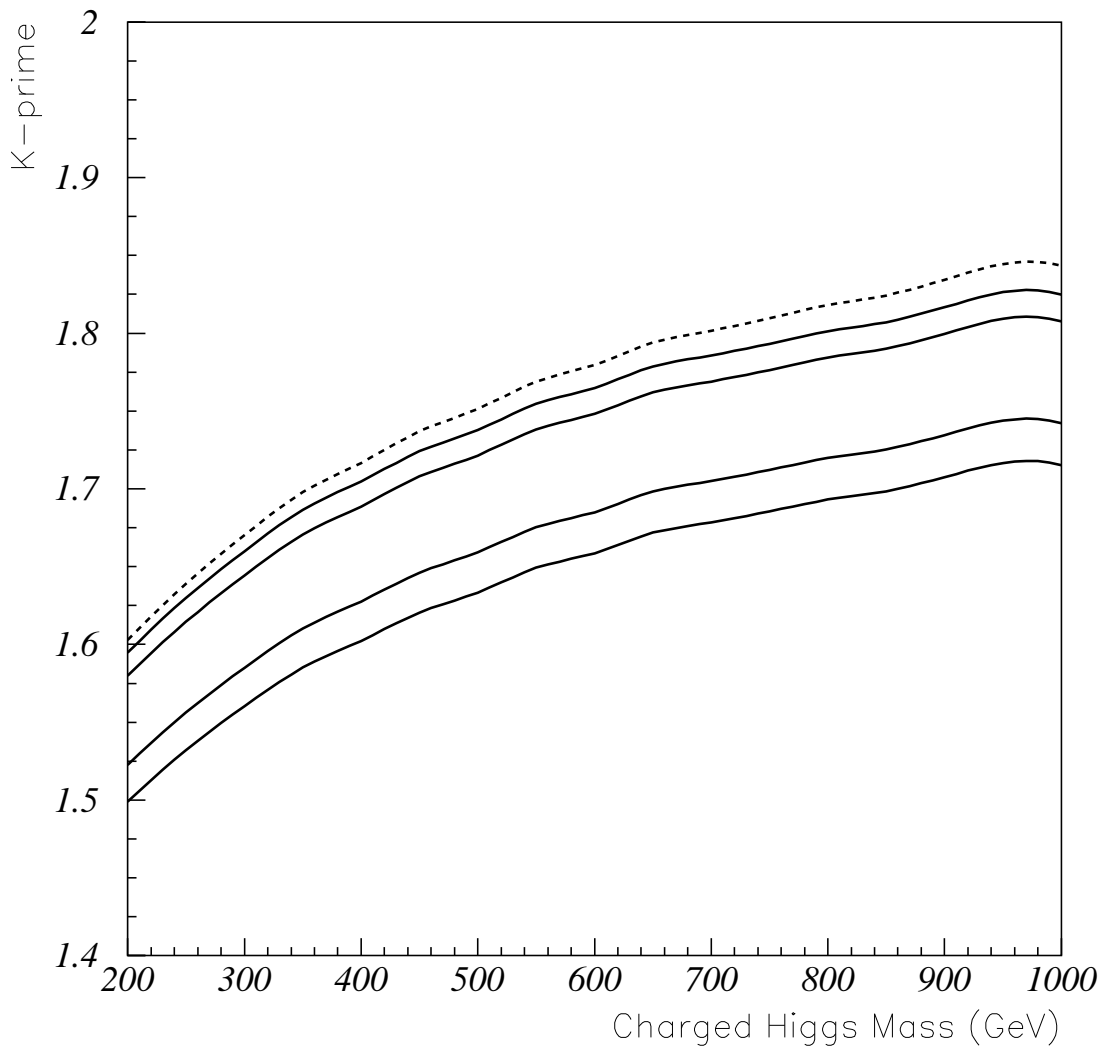


FIG. 7. K' (defined in text) as a function of charged Higgs boson mass with $\tan \beta = 2, 5, 10, 30$ (solid lines from top to bottom) and $\mu = \mu_0$. The dashed line is K-factor in Fig. 6 which is re-shown for comparison.